

*Generalizable Features of Interfacial Water Structure Predict the Hydrophobicity of Chemically Heterogeneous Surfaces*

**Authors:**

Bradley C. Dallin, Atharva S. Kelkar, and Reid C. Van Lehn\*

Department of Chemical and Biological Engineering, University of Wisconsin – Madison, Madison, WI, 53706, USA.

**Corresponding author:**

Reid C. Van Lehn

1415 Engineering Drive, Madison, WI 53706

(608) 263-9487

vanlehn@wisc.edu

## **Abstract**

The hydrophobicity of an interface determines the magnitude of hydrophobic interactions that drive numerous biological and industrial processes. Chemically heterogeneous interfaces are abundant in these contexts; examples include the surfaces of proteins, functionalized nanomaterials, and polymeric materials. While the hydrophobicity of nonpolar solutes can be predicted and related to the structure of interfacial water molecules, predicting the hydrophobicity of chemically heterogeneous interfaces remains a challenge because of the complex, non-additive contributions to hydrophobicity that depend on the chemical identity and nanoscale spatial arrangements of polar and nonpolar groups. In this work, we utilize atomistic molecular dynamics simulations in conjunction with enhanced sampling and data-centric analysis techniques to quantitatively relate changes in interfacial water structure to the hydration free energies (a thermodynamically well-defined descriptor of hydrophobicity) of chemically heterogeneous interfaces. We analyze a large data set of 58 self-assembled monolayers (SAMs) containing ligands with nonpolar and polar end groups of different chemical identity (amine, amide, and hydroxyl) in five mole fractions, two spatial patterns, and with scaled partial charges. We find that only five features of interfacial water structure are required to accurately predict hydration free energies. Examination of these features reveals mechanistic insights into the interfacial hydrogen bonding behaviors that distinguish different surface compositions and patterns. This analysis also identifies the probability of highly coordinated water structures as a unique signature of hydrophobicity. These insights provide a physical basis to understand the hydrophobicity of chemically heterogeneous interfaces and connect hydrophobicity to experimentally accessible perturbations of interfacial water structure.

## Introduction

The hydrophobicity of an interface reflects its thermodynamic tendency to minimize contact with surrounding water molecules and determines the magnitude of water-mediated hydrophobic interactions. Hydrophobic interactions between homogeneous nonpolar solutes in water have been extensively studied and the relationship between interfacial hydrophobicity and the scale-dependent structuring of water near nonpolar domains has been validated by experiment and simulation.<sup>1-4</sup> In contrast, the hydrophobicity of interfaces that are chemically heterogeneous at the nanoscale — *i.e.*, interfaces with nonpolar and polar groups in close ( $\sim$ nm) proximity — is poorly understood and difficult to predict.<sup>5-9</sup> This knowledge gap is significant because hydrophobic interactions with chemically heterogeneous interfaces are central to wide-ranging industrial and biological processes, such as polypeptide folding,<sup>10, 11</sup> protein interactions,<sup>12-15</sup> non-specific protein adsorption,<sup>16-18</sup> cellular uptake,<sup>19, 20</sup> and chromatographic separations.<sup>21, 22</sup> As a result, substantial experimental, theoretical, and computational efforts have sought to understand how the polar groups, when placed adjacent to nonpolar domains, impact interfacial hydrophobicity and the associated structure of water.<sup>23-30</sup>

Approaches to quantify the hydrophobicity of chemically heterogeneous interfaces typically assume that contributions to hydrophobicity are additive. For example, interfacial hydrophobicity is often estimated based on the amount of nonpolar solvent-accessible surface area<sup>31-35</sup> or by group-specific parameters such as hydrophobicity scale values<sup>36</sup> or octanol-water partition coefficients.<sup>19, 37, 38</sup> However, these methods neglect perturbations to water structure by polar groups near nonpolar domains that lead to cooperative, non-additive contributions to hydrophobicity,<sup>24-26, 39</sup> as highlighted by recent experimental measurements of hydrophobic forces with chemically heterogeneous interfaces.<sup>27-29</sup> In these experiments, adhesion forces were

measured between an atomic force microscope (AFM) tip functionalized with a nonpolar self-assembled monolayer (SAM) and planar gold substrates functionalized with mixed SAMs containing both nonpolar and polar ligand end groups. The difference between adhesion forces measured in water and in methanol was identified as the hydrophobic force.<sup>27-29</sup> Comparing hydrophobic forces for different mixed SAM compositions indicated that replacing amine end groups that are adjacent to a nanoscale nonpolar domain with amide groups can weaken and even eliminate hydrophobic forces.<sup>28</sup> Related experimental measurements similarly revealed that hydrophobic forces between a nonpolar AFM tip and  $\beta$ -peptide oligomers containing well-defined nonpolar and polar domains were modulated by the chemical identity of the polar group and followed similar trends as for the mixed SAMs.<sup>27, 28</sup> Conversely, hydrophobic forces were eliminated for structural isomers of the same  $\beta$ -peptide oligomers in which polar and nonpolar groups were interspersed without a well-defined nonpolar domain. These findings underscore that both the chemical identity of polar groups and the nanoscale spatial arrangement (*i.e.*, patterning) of polar and nonpolar groups at chemically heterogeneous interfaces substantially influence interfacial hydrophobicity.<sup>28</sup>

To complement experimental studies, atomistic molecular dynamics (MD) simulations have been utilized to study relationships between interfacial water structure and the thermodynamic driving forces underlying hydrophobic assembly,<sup>3, 23, 40</sup> enabling effective predictions of protein-ligand binding,<sup>13, 41</sup> protein-protein interactions,<sup>30</sup> and biomolecule aggregation.<sup>42</sup> Similar simulations have found that patterning influences the thermodynamics of the hydration layer near chemically heterogeneous surfaces.<sup>43, 44</sup> To compare the hydrophobicity of different surfaces, simulation studies have also identified the magnitude of water density fluctuations as a descriptor of interfacial hydrophobicity.<sup>45-49</sup> Water density fluctuations are

enhanced near hydrophobic surfaces, increasing the probability that a cavity near the interface spontaneously dewets. This probability can be quantified as a corresponding hydration free energy<sup>45-49</sup> which captures correlations between interfacial water molecules and has been shown to effectively predict binding interactions on proteins.<sup>30,50</sup> By calculating hydration free energies, we previously determined that molecular-level order modulates the hydrophobicity of uniformly nonpolar SAMs by perturbing interfacial water structure, in agreement with similar trends identified through experimental hydrophobic force measurements.<sup>29, 51, 52</sup> This accumulated research establishes strong connections between interfacial hydrophobicity, variations in the properties of homogeneous and chemically heterogeneous interfaces, and interfacial water structure. However, these connections remain largely qualitative, and systematic studies to relate perturbations to interfacial water structure to the hydrophobicity of chemically heterogeneous interfaces are lacking.

In this work, we hypothesize that descriptors of interfacial water structure can be quantitatively related to the hydrophobicity of chemically heterogeneous interfaces. To test this hypothesis, we utilize atomistic MD simulations to calculate water structural order parameters and hydration free energies for a large set of SAMs containing amine, amide, and hydroxyl polar groups in various surface compositions and patterns. Using a feature selection workflow, we find that only five water structural features are important to accurately predict SAM hydration free energies. Analysis of these five features provides a physical basis for understanding how surface properties modulate the hydration free energy – and thus hydrophobicity - by altering the hydrogen bond network and orientation of interfacial water molecules. These results produce new understanding of perturbations to water structure at chemically heterogeneous surfaces which can be extrapolated to more complex materials like proteins and peptides.

## Results and Discussion

*Hydration free energy calculations capture experimental trends.* To understand how polar end groups modulate interfacial hydrophobicity, we first simulated the set of alkanethiol SAMs that were shown in Ref. 28 to exhibit substantially different hydrophobic interactions in prior AFM experiments. This set includes single-component SAMs in which ligands were functionalized with either nonpolar (methyl) or polar (amine or amide) end groups and mixed SAMs in which 40% of the ligands were functionalized with polar end groups and 60% of the ligands were functionalized with nonpolar end groups (Figure 1A).<sup>28</sup> While the end group pattern is unknown in the experiments, we modeled fully separated SAM patterns because analogous experiments have shown that  $\beta$ -peptide oligomers only exhibit large deviations in hydrophobicity when they have well-defined separated polar and nonpolar domains.<sup>27, 28</sup> This data set permits initial simulation interrogation of homogeneous and chemically heterogeneous surfaces for comparison to experimental trends.

For each SAM, we performed Indirect Umbrella Sampling (INDUS) to compute the hydration free energy ( $\mu_v$ ), or excess chemical potential, of a  $2.0 \times 2.0 \times 0.3$  nm<sup>3</sup> cuboidal cavity (denoted by the subscript  $v$ ) near the SAM-water interface (see Methods).  $\mu_v$  reports on the magnitude of water density fluctuations within the cavity that emerge from the collective interactions of water molecules with each other and with the SAM. Smaller values of  $\mu_v$  (corresponding to enhanced fluctuations) indicate a more hydrophobic interface. Although  $\mu_v$  will depend on the size and placement of the cavity,  $\mu_v$  can be used as a thermodynamically well-defined descriptor to compare the interfacial hydrophobicity of different surfaces if the cavity is consistently defined.<sup>53</sup> Past studies of SAMs have shown that  $\mu_v$  correlates with equilibrium water contact angles<sup>45, 54</sup> and experimentally measured hydrophobic forces.<sup>51</sup> Similarly, Figure 1B

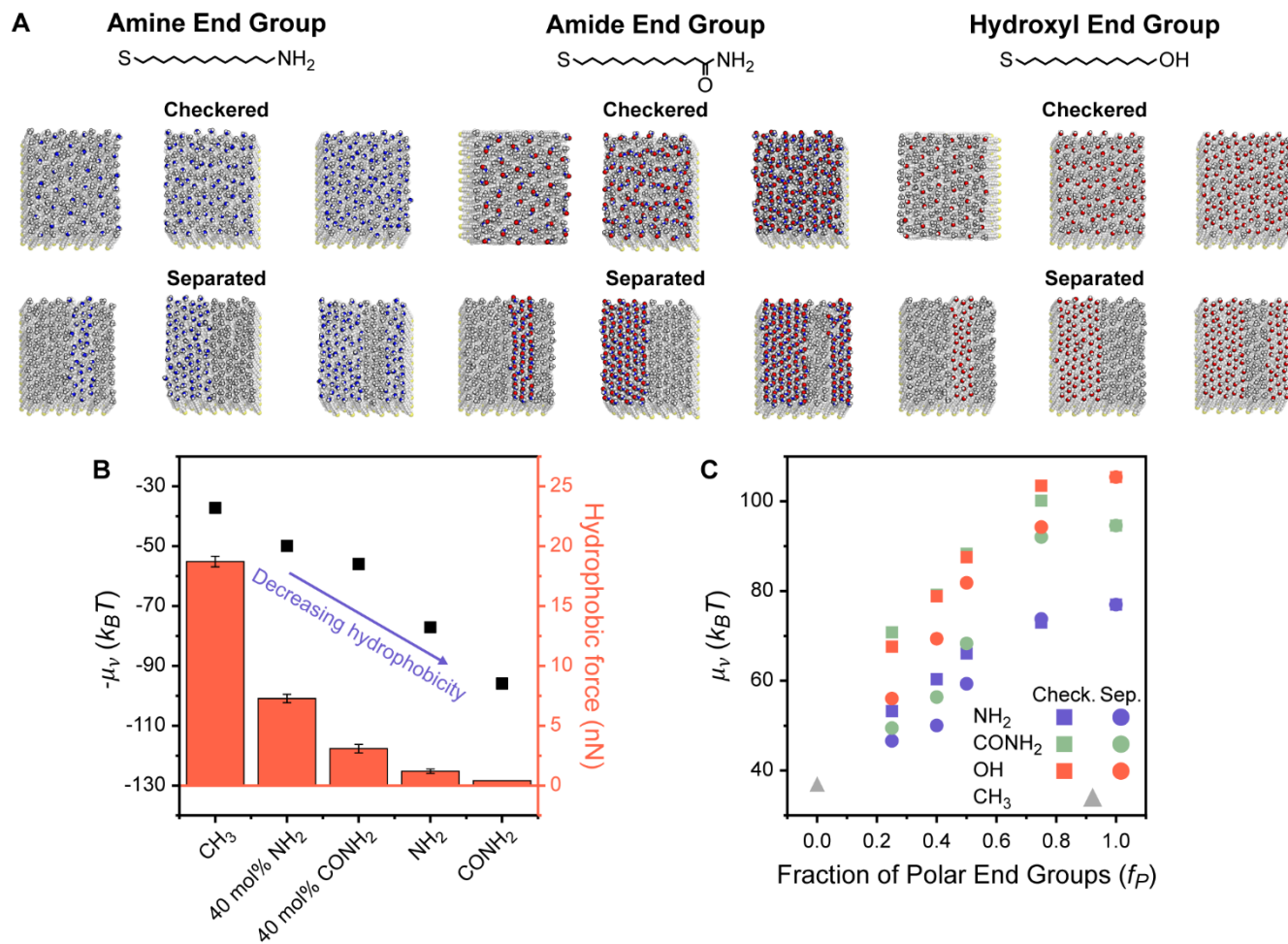


**Figure 1.** (A) Chemical structures and top-down simulation snapshots of SAMs with amine, amide, and hydroxyl end groups in checked and separated patterns and  $f_p = 0.25, 0.50,$  and  $0.75$  mole fractions. (B) Comparison between hydration free energies ( $\mu_v$ ) measured by INDUS (black squares) and hydrophobic forces measured by AFM experiments (red columns). Experimental hydrophobic force data are adapted from Wang *et al.*<sup>28</sup>.  $-\mu_v$  is plotted to illustrate the trend relative to the experimental values. (C) Hydration free energies as a function of the mole fraction of polar end groups ( $f_p$ ) for the checked (squares) and separated (circles) patterned SAMs.

illustrates that  $\mu_v$  values computed for this set of SAMs are negatively correlated with hydrophobic forces measured experimentally in Ref. 28, confirming that smaller values of  $\mu_v$  correspond to SAMs that appear more hydrophobic in experiments. In particular, the simulations reproduce the finding that mixed SAMs with amide-functionalized ligands are less hydrophobic than mixed SAMs with amine-functionalized ligands. This result demonstrates that our simulation model qualitatively reproduces the effects of polar end group chemistry on SAM hydrophobicity, supporting further investigation into the origin of these effects.

To test the hypothesis that surface chemistry uniquely modulates hydrophobicity by perturbing interfacial water structure, we expanded the set of simulated SAMs to include mixed SAMs with amine-, amide-, and hydroxyl-functionalized ligands with six different mole fractions of polar end groups ( $f_p$ ) and two different patterns (“checkered” and “separated”). We also considered homogeneous SAMs in which the end group partial charges were scaled to fully span the range of possible  $\mu_v$  values for each end group.<sup>23, 55</sup> In total, we studied 58 SAMs to provide a large data set for further analysis. Figure 1A shows representative SAMs for each chemistry, composition, and pattern, with additional details included in Section S1 of the Electronic Supporting Information (ESI). For each SAM, we computed  $\mu_v$  using INDUS (Figure 1C) to quantify interfacial hydrophobicity and computed a set of water order parameters from a complementary unbiased MD simulation to quantify the structure of interfacial water molecules (defined as water molecules within 0.3 nm of the SAM-water interface). These order parameters include information on SAM-SAM, SAM-water, and water-water hydrogen bonds, water orientations relative to the SAM, and the water triplet angle (*i.e.*, the angle formed between an interfacial water molecule and two neighboring water molecules).<sup>56-58</sup> ESI Section S2 provides a full description for each parameter and ESI Figures S7-12 show variations in these parameters for



different SAMs. Subsets of these parameters have been used previously to understand how peptide side chain chemistry affects binding,<sup>57</sup> surface polarity alters interfacial water orientation,<sup>23</sup> and SAM order affects hydrophobic interactions.<sup>52</sup> However, quantifying which order parameters are most important for predicting hydrophobicity across a broad range of SAMs is challenging through traditional approaches that investigate single parameters independently.

***Data-centric analysis identifies important water structural features.*** We implemented a data-centric workflow to relate interfacial water order parameters to interfacial hydrophobicity quantitatively. We defined a set of 152 features that were each related to a particular value of an order parameter; for example, the probability of observing zero water-water hydrogen bonds is a feature. Each of the 58 SAMs was associated with a feature vector containing normalized numerical values for all features (determined from the unbiased MD simulation) and a single value of  $\mu_v$ . We then developed a three-step workflow to select the minimum set of features required to accurately predict  $\mu_v$ , and, thus, interfacial hydrophobicity (Figure 2A). In the first step, we reduced the number of features by computing the Pearson's correlation coefficient between all pairs of features and removing features that were above a correlation threshold (ESI Section S2). In the second step, we performed Lasso regression using the 45 remaining uncorrelated features (ESI Table S2) for each SAM as input to predict corresponding values of  $\mu_v$ . In the final step, we performed 5-fold cross validation using multiple linear regression to relate the minimum set of features identified from Lasso regression to  $\mu_v$ , thereby determining the overall accuracy of our approach. This entire approach (including INDUS and unbiased simulations) was repeated three times for independent sample sets to ensure robustness and estimate simulation error.

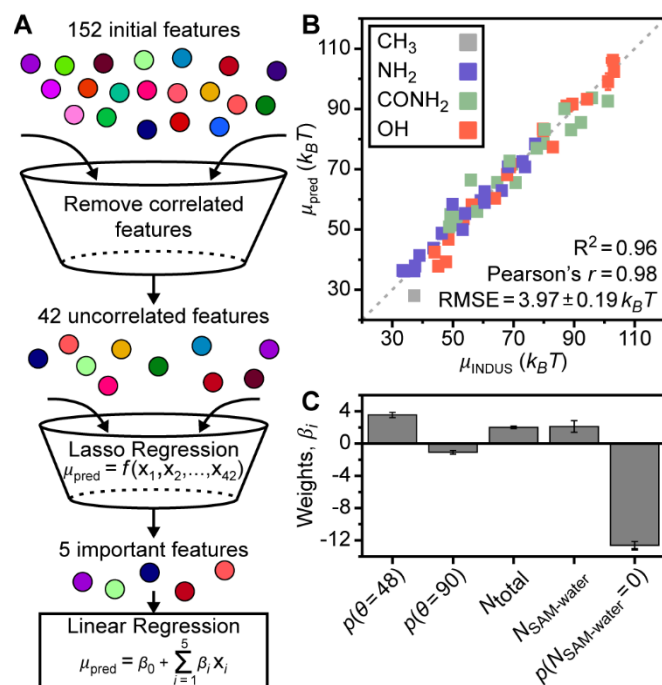


**Figure 2.** (A) Schematic of feature selection workflow. (B) Parity plot comparing hydration free energies ( $\mu_v$ ) predicted from multivariate linear regression to those calculated by INDUS. Each point is the prediction for the SAM when it is included in the validation set during 5-fold cross validation, such that the SAM is not included in model training. Error bars are smaller than the symbols. (C) Comparison of feature weights for the linear regression model. Error bars were calculated as the standard deviation of the weights from three independent repetitions of the simulation and feature selection workflow.

Strikingly, we found that only five features are required to accurately predict the full range of SAM hydration free energies even though the SAM data set contains both homogeneous and chemically heterogeneous SAMs with different compositions, patterns, and end group chemistries, and contains SAMs with scaled end group partial charge (ESI Section S2), suggesting that the selected features may be universally relevant to SAM hydrophobicity. The five features, listed in order of model prediction importance (discussed below), are the probability that an interfacial water molecule forms zero SAM-water hydrogen bonds,  $p(N_{\text{SAM-water}} = 0)$ , the probability that

an interfacial water molecule forms a triplet angle of  $48^\circ$ ,  $p(\theta = 48^\circ)$ , the average total number of hydrogen bonds per molecule (ligand with a polar end group or water),  $N_{\text{total}}$ , the average number of SAM-water hydrogen bonds,  $N_{\text{SAM-water}}$ , and the probability that an interfacial water molecule forms a triplet angle of  $90^\circ$ ,  $p(\theta = 90^\circ)$ . Figure 2B shows a parity plot comparing  $\mu_v$  values predicted by the final linear regression model to those computed by INDUS. The linear regression model has an RMSE of  $3.97 \pm 0.19 \text{ } k_B T$ . For comparison, INDUS calculations have a replica error of about  $2 \text{ } k_B T$ , indicating that the predictions are quite accurate. Predicted  $\mu_v$  values are also strongly correlated with INDUS values with a Pearson's  $r$  of 0.98 (a value of 1.0 indicates perfect linear correlation). We further performed 5-fold cross validation using Lasso regression and separately utilized a nonlinear Random Forest model with recursive feature elimination to select features for the same data set (ESI Section S2). Both approaches identified similar features, indicating the robustness of model findings. Figure 2C compares the weights of the coefficients from the linear regression model to quantify their relative importance. These results show that  $p(N_{\text{SAM-water}} = 0)$  is the most important feature in the model, followed by  $p(\theta = 48^\circ)$ .  $N_{\text{total}}$  and  $N_{\text{SAM-water}}$  of are comparable importance and  $p(\theta = 90^\circ)$  is least important. These five features, and their physical significance, are described in detail in the sections below.

***SAM-water hydrogen bonding strongly correlates with hydrophobicity.*** Two of the features identified as strong predictors of hydrophobicity,  $p(N_{\text{SAM-water}} = 0)$  and  $N_{\text{SAM-water}}$ , quantify the formation of hydrogen bonds between the SAM and interfacial water molecules. The feature that has the highest weight in the linear regression model (and hence contributes most substantially to model predictions) is  $p(N_{\text{SAM-water}} = 0)$ ; large values of  $p(N_{\text{SAM-water}} = 0)$  indicate that water molecules are unlikely to form hydrogen bonds with the SAM and that the SAM is

accordingly more hydrophobic. This feature is thus a simple, intuitive descriptor for SAM hydrophobicity that is conceptually related to water density fluctuations because the enhancement of such fluctuations near more hydrophobic surfaces is due to weak surface-water interactions.<sup>45</sup>

47

To determine if this feature alone can capture trends in SAM hydrophobicity, Figure 3A plots  $\mu_v$  versus  $p(N_{\text{SAM-water}} = 0)$  for the SAM data set. For this comparison (and the comparisons in the following sections), homogeneous SAMs with scaled partial charges are omitted to determine how features correlate with the hydrophobicity of chemically heterogeneous SAMs with different ligand end groups, values of  $f_p$ , and patterns.  $\mu_v$  and  $p(N_{\text{SAM-water}} = 0)$  are highly correlated with a Pearson's  $r$  of -0.95; the negative correlation is expected because larger values of  $p(N_{\text{SAM-water}} = 0)$  indicate a more hydrophobic surface with lower  $\mu_v$ . Linear regression with only this feature predicts  $\mu_v$  with an RMSE of  $5.86 \pm 0.07 k_B T$ , demonstrating that this feature alone provides reasonable prediction accuracy but including the other four features reduces the prediction RMSE by approximately  $2 k_B T$ . The other important feature based on SAM-water hydrogen bonds is  $N_{\text{SAM-water}}$ . Figure 3B shows that this feature also has a linear correlation with hydration free energy and a Pearson's  $r$  of 0.95. In contrast to  $p(N_{\text{SAM-water}} = 0)$ , this feature quantifies favorable interactions between interfacial water molecules and the SAM, with larger values indicating more water molecules on average bound to the SAM. These two features provide complementary information on SAM-water interactions and demonstrate that analysis of hydrogen bonding can serve as a baseline prediction of trends in  $\mu_v$ . However, Figure 3A also shows systematic deviations in predictions for different end groups and patterns: for example,  $\mu_v$  is underpredicted for SAMs with amine end groups and overpredicted for separated patterns compared to checkered patterns. Accordingly, we investigated the physical origin of the

other important features identified by our workflow to determine why they lead to the more accurate predictions shown in Figure 2.

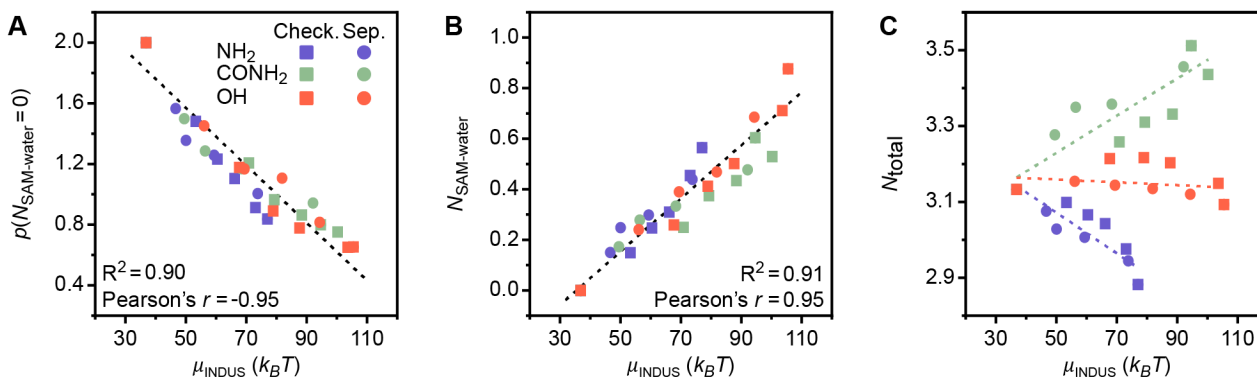


**Figure 3.** Unnormalized values of features related to interfacial hydrogen bonding for the checked (squares) and separated (circles) SAMs versus hydration free energies ( $\mu_v$ ). Values for SAMs with amine (purple), amide (green), and hydroxyl (orange) end groups are plotted separately. (A) Probability density for zero SAM-water hydrogen bonds formed by an interfacial water molecule. The black dotted line is a linear fit to all data. (B) Number of hydrogen bonds between SAM polar end groups and interfacial water molecules. (C) Total number of hydrogen bonds formed by an interfacial water molecule. Each value is averaged over all interfacial water molecules and simulation time. The dotted lines are linear fits for each end group (including both checked and separated patterns).

***Total interfacial hydrogen bonds vary with polar group chemistry.*** Another important feature that depends on hydrogen bonds is  $N_{\text{total}}$ , which quantifies the total number of SAM-water, water-water, and SAM-SAM hydrogen bonds per molecule. Increased SAM-water hydrogen bonds, as described in the previous section, indicate strong SAM-water interactions that decrease interfacial hydrophobicity. Increased interfacial water-water hydrogen bonds signify a more connected hydrogen bond network, or a more ordered interfacial water structure, which has been linked to

decreased hydrophobicity for idealized nonpolar solutes<sup>3</sup> and SAMs.<sup>52</sup> Increased SAM-SAM hydrogen bonds could indicate fewer hydrogen bonding donor or acceptor sites available for SAM-water hydrogen bonding, consequently increasing interfacial hydrophobicity. Thus, this feature encodes information on a range of possible behaviors with distinct contributions to interfacial hydrophobicity that could vary for different SAM properties.

Figure 3C plots  $\mu_v$  versus  $N_{\text{total}}$  following the previous approach in Figures 3A and 3B. Different trends are observed for each polar end group; notably,  $\mu_v$  scales approximately linearly with  $N_{\text{total}}$  for each polar end group separately but with substantially different slopes. The difference in scaling suggests that  $N_{\text{total}}$  can distinguish between polar end group chemistries in the linear regression model (Figure 2B); that is, the relative contribution of this feature to the predicted value of  $\mu_v$  differs between polar end groups. Figure 4 shows variations in the average number of SAM-SAM, SAM-water, and water-water hydrogen bonds that contribute to  $N_{\text{total}}$ . For all three end groups, variations in  $N_{\text{total}}$  reflect the competition between increased SAM-water and decreased water-water hydrogen bonds as  $f_p$  increases (leading to an increase in  $\mu_v$ ). These general trends can be interpreted in terms of the disruption of water structure near a uniformly nonpolar surface (for the lowest value of  $\mu_v$ ) by the presence of polar groups that can interact favorably with interfacial water molecules. For the SAMs containing amine end groups, SAM-water hydrogen bonding is relatively weak and consequently the increase in SAM-water hydrogen bonds is insufficient to compensate for the decrease in water-water hydrogen bonds, leading to a decrease in  $N_{\text{total}}$  as  $\mu_v$  increases. Conversely,  $N_{\text{total}}$  is nearly constant with  $\mu_v$  for SAMs containing hydroxyl end groups because the increase in the number of favorable SAM-water hydrogen bonds compensates for the decrease in number the water-water hydrogen bonds.

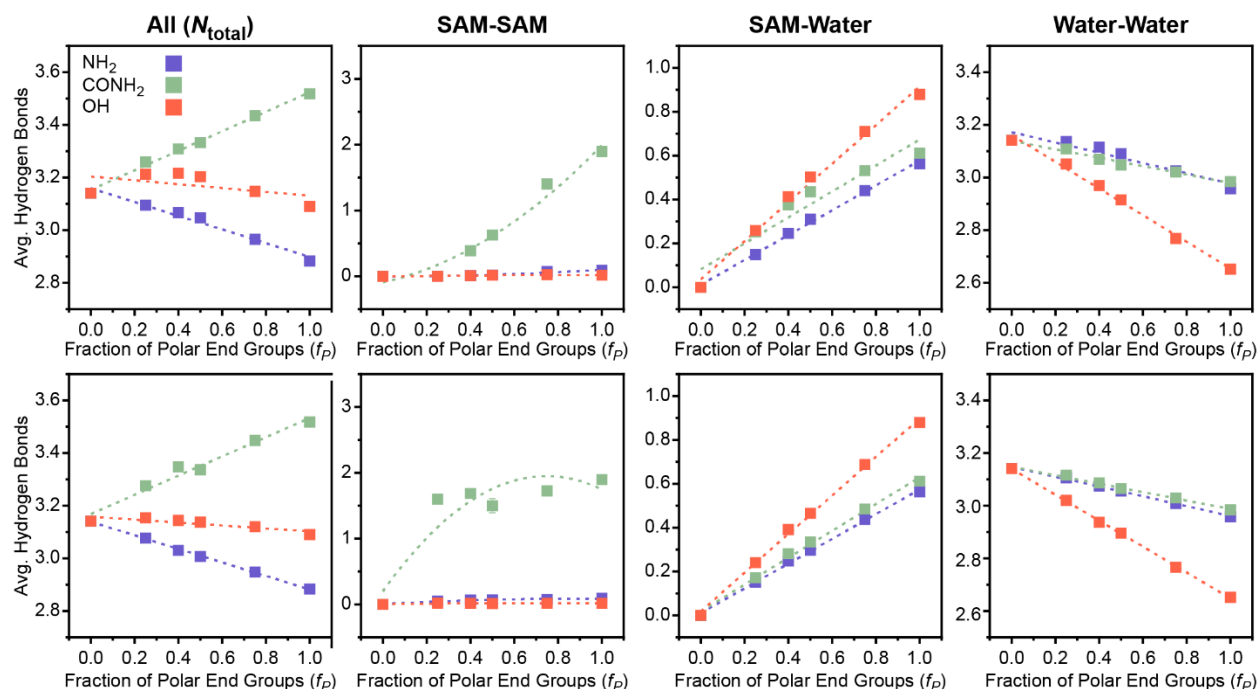


**Figure 4.** Average number of hydrogen bonds per molecule (excluding ligands with methyl end groups that cannot form hydrogen bonds) for all hydrogen bonds ( $N_{total}$ ), SAM-SAM hydrogen bonds, SAM-water hydrogen bonds, and water-water hydrogen bonds. Top row: hydrogen bonds for checkered SAMs. Bottom row: hydrogen bonds for separated SAMs.

The SAMs containing amide end groups exhibit similar trends as the SAMs containing amine end groups. However, these SAMs are unique because only the amide end groups form a significant number of SAM-SAM hydrogen bonds (Figure 4) which increases with increasing  $f_p$  and contributes to an overall increase in  $N_{total}$  with  $\mu_v$  (for SAMs in the checkered pattern; because the total number of hydrogen bonds is normalized by the number of polar end groups, SAM-SAM hydrogen bonds remain relatively constant for the amide-containing SAMs in the separated pattern since the local chemical environment does not change with  $f_p$ ). Intra-surface hydrogen bonding has been shown to reduce surface hydrophilicity in prior simulation studies of

model surfaces,<sup>59</sup> which explains why amide end groups contribute to lower values of  $\mu_v$  than hydroxyl end groups (on average) despite larger values of  $N_{\text{total}}$ . This behavior may also explain why  $\mu_v$  for the checkered SAM with 75 mol% amide end groups is larger than  $\mu_v$  for a homogeneous SAM with only amide end groups.

Together, this analysis indicates that  $N_{\text{total}}$  captures variations in hydrogen bonding behavior that depend on the chemical identity of SAM polar end groups and points to physical mechanisms underlying variations in SAM hydrophobicity. Incorporation of this feature into the linear regression model provides information to distinguish the influence of end group chemistry in predictions of  $\mu_v$ . Moreover, the ability to identify a single feature (rather than a subset of additional features related to the variation of each type of hydrogen bond separately) that quantitatively relates these complex behaviors to  $\mu_v$  is a benefit of our data-centric workflow.

***Orientational features encode information on crowded water coordination shells.*** The feature with the largest positive weight in the final linear regression model (Figure 2C) is  $p(\theta = 48^\circ)$ , which is the probability that an interfacial water molecule forms a triplet angle of  $48^\circ$ . The triplet angle is calculated by measuring the angle between an interfacial water molecule and its two nearest neighbors within a 0.33 nm radius. Figure 5A illustrates differences in the triplet angle distribution for SAMs with varying fractions of polar end groups, hinting at the ability of this distribution to distinguish surfaces with varying HFEs. While these distributions vary substantially, the importance of variations to  $p(\theta = 48^\circ)$  identified by the feature selection workflow indicates that this probability provides unique information not directly quantified by features associated with hydrogen bonding and thus merits further analysis. Figure 5B plots  $\mu_v$  versus  $p(\theta = 48^\circ)$ . Like  $N_{\text{total}}$ ,  $p(\theta = 48^\circ)$  exhibits different variations with respect to  $\mu_v$  for



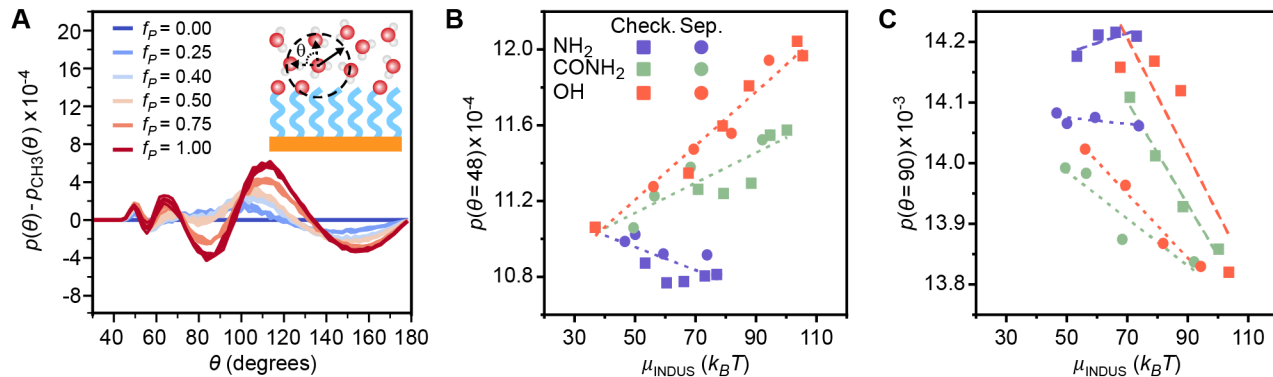


**Figure 5.** (A) Schematic of the calculation of the water triplet angle and example distributions for “checkered” SAMs with amine end groups as a function of the fraction of polar end groups ( $f_p$ ). Distributions show the difference relative to a SAM containing only methyl end groups, which corresponds to  $f_p=0.00$ . (B) Probability density for an interfacial water molecule forming a triplet angle,  $\theta$ , of  $48^\circ$  for the checkered (squares) and separated (circles) SAMs versus hydration free energies ( $\mu_\nu$ ). (D) Probability density for an interfacial water molecule forming a triplet angle of  $90^\circ$ . The dashed lines and dotted lines are linear fits for the checkered and separated SAMs, respectively, for each end group.

different polar end groups and thus provides information to the regression model to distinguish between SAMs with different end groups.  $p(\theta = 48^\circ)$  increases with  $\mu_\nu$  for SAMs containing amide and hydroxyl end groups and decreases with  $\mu_\nu$  for SAMs containing amine end groups, which follows a similar pattern as  $N_{\text{total}}$ . While trends in the formation of hydrogen bonds have a clear physical interpretation, the physical significance of this feature is less clear. Monroe and Shell have suggested that a small peak in the triplet angle distribution at around  $50^\circ$  arises due to a fifth neighbor in the coordination shell of bulk water.<sup>58</sup> However, it is unclear how interfaces and surface properties affect this feature.

To investigate the origin of the  $p(\theta = 48^\circ)$  feature, we calculated the water coordination number,  $C_N$ , by counting the number of heavy atoms within 0.33 nm of the oxygen atom of an

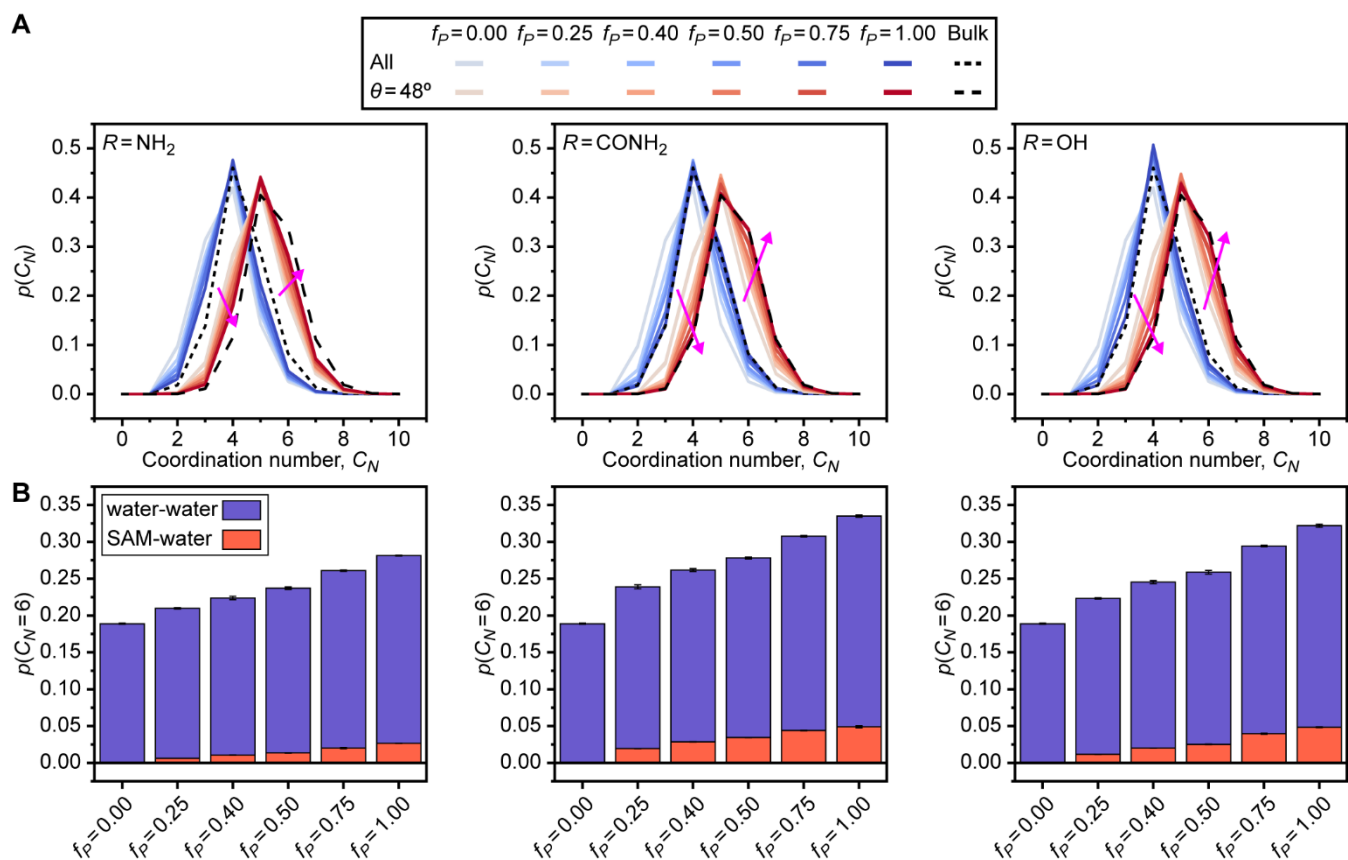


**Figure 6.** (A) Water coordination number ( $C_N$ ) probability density functions for all interfacial water molecules (blue lines) and only interfacial water molecules with a triplet angle of  $48^\circ$  (red lines). Bulk water probability density functions for all water molecules (dotted line) and water molecules with a triplet angle of  $48^\circ$  (dashed line) are included for reference. Shifts with increasing  $f_p$  are indicated by the purple arrows. (B) Probability density function values for  $C_N = 6$ . Stacked columns indicate the contributions from water-water coordination (blue columns) and SAM-water coordination (red columns). A and B both consider only checked SAMs.

interfacial water molecule. Figure 6A compares the probability distribution of the coordination number,  $p(C_N)$ , when calculated separately for all water molecules (*i.e.*, all possible triplet angles) and for only those water molecules with a triplet angle of  $48^\circ$ . Results are presented for bulk water

and for the checkered SAMs as a function of  $f_p$ ; the separated SAMs follow approximately the same trend (ESI Figure S21). As previously suggested,<sup>58</sup>  $p(C_N)$  for water molecules with a triplet angle of  $48^\circ$  is shifted toward larger values of  $C_N$ , with a maximum at  $C_N = 5$ , for all SAMs and for bulk water. This finding indicates that  $p(\theta = 48^\circ)$  captures information on the likelihood of observing highly coordinated water structures. We note that  $p(\theta = 48^\circ)$  is very small for bulk water, so the observation of these highly coordinated structures is rare. Compared to bulk water, all  $p(C_N)$  distributions are shifted toward small values of  $C_N$  when  $f_p$  is low, reflecting the vapor-like arrangement of water molecules near more hydrophobic surfaces.<sup>60</sup> Increasing  $f_p$  shifts all distributions toward those of bulk water, which is consistent with an increase in the hydrophilicity of the surface. These shifts are less pronounced for SAMs with amine end groups due to the general decrease in hydrogen bonds for SAMs with amine end groups (Figure 3B). The difference in these shifts between different polar groups highlights that  $p(\theta = 48^\circ)$  hence contains information on end group contributions to the formation of highly coordinated water structures.

The shift toward higher coordination numbers suggests that the polar end groups either interact directly with water molecules at the interface (thereby increasing their coordination numbers) or nucleate highly coordinated water structures near more polar SAMs. We tested both possibilities by separately calculating water-water and SAM-water contributions to  $p(C_N = 6)$  because the  $p(C_N)$  distributions for the SAMs containing amide and hydroxyl groups have a shoulder at  $C_N = 6$  when  $f_p$  is large. Figure 6B shows that the increase in  $p(C_N = 6)$  as  $f_p$  increases is largely driven by the water-water contribution for all checkered SAMs. This result indicates that the polar groups nucleate highly coordinated water structures at the interface. As a secondary effect, we also find a substantial SAM-water contribution to  $p(C_N = 6)$  for the SAMs containing amide and hydroxyl end groups, indicating that the strong interactions between these polar end

groups and interfacial water molecules lead to crowded coordination shells that are rarely observed in bulk water. Together, this analysis indicates that  $p(\theta = 48^\circ)$  encodes information on the formation of highly coordinated water structures that are nucleated near more hydrophilic SAMs and are thus signatures of hydrophilic surfaces.

***Disordered arrangements of molecules differentiate SAM patterns.*** The  $p(\theta = 90^\circ)$  feature has the smallest weight of the important features (Figure 2C) but plays an important role in distinguishing SAMs with different patterns. Figure 5C plots  $p(\theta = 90^\circ)$  versus  $\mu_v$  and reveals that SAMs with checkered and separated patterns exhibit substantially different variations in the scaling of  $p(\theta = 90^\circ)$  with  $\mu_v$ . The physical significance of this feature can be inferred from the peak at  $90^\circ$  in the triplet angle distribution of an ideal gas (ESI Section S3), which indicates that large values of  $p(\theta = 90^\circ)$  are characteristic of disordered, gas-like arrangements of water molecules. Prior simulation studies have shown that water structure near hydrophobic surfaces exhibits similarities to the water-vapor interface,<sup>60</sup> which is consistent with our finding that more hydrophobic SAMs (smaller  $\mu_v$ ) have larger values of  $p(\theta = 90^\circ)$ . The differences in behavior between checkered and separated SAMs can be attributed to the larger hydrophobic domains associated with separated patterns. ESI Figure S20 shows that  $p(\theta = 90^\circ)$  increases near these hydrophobic domains but is lower on average for checkered surfaces with the same value of  $f_P$ , reflecting the pinning of the water-vapor interface when polar groups are uniformly distributed across the SAM. This finding is consistent with prior simulation studies<sup>26, 51</sup> and indicates that  $p(\theta = 90^\circ)$  quantifies the formation of large hydrophobic domains found in certain SAM patterns.

## Conclusions

We computed hydration free energies (as quantitative descriptors of interfacial hydrophobicity) and water structural parameters for 58 SAMs, encompassing variations in polar group chemistries, compositions, and spatial patterns, using MD simulations. Lasso regression revealed that only five water structural features were needed to quantitatively predict SAM hydration free energies with an accuracy comparable to that of rigorous enhanced sampling calculations. We investigated the physical significance of the five features identified and their importance in distinguishing different SAM properties. Two features — the probability that an interfacial water molecule forms zero SAM-water hydrogen bonds and the average total number of SAM-water hydrogen bonds — correlated strongly with SAM hydrophobicity and contribute substantially to the regression model. Consequently, analysis of SAM-water hydrogen bonding alone provides a baseline prediction for hydrophobicity that can be intuitively understood as quantifying the strength of SAM-water interactions. Two additional features — the average total number of hydrogen bonds per molecule and the probability that an interfacial water molecule forms a triplet angle of  $48^\circ$  — were necessary to distinguish contributions to hydrophobicity from different polar groups. The average total number of hydrogen bonds per molecule captured variations in SAM-water, SAM-SAM, and water-water hydrogen bonding in analogy to the restructuring of hydrogen bond networks that underlies the hydrophobicity of nonpolar solutes. The probability that an interfacial water molecule forms a triplet angle of  $48^\circ$  quantifies the formation of highly coordinated interfacial water structures as a unique, previously unreported signature of hydrophilic surfaces. The last feature, the probability that an interfacial water molecule forms a triplet angle of  $90^\circ$ , distinguishes nanoscale spatial patterns by capturing disordered arrangements of water molecules near large nonpolar domains.

These findings establish a link between variations in water structure and hydrophobicity for chemically heterogeneous interfaces. Typical experimental approaches can directly quantify hydrophobic interactions for simple systems (*e.g.* planar interfaces<sup>28, 29, 61</sup>) or approximate interfacial hydrophobicity based on additive approximations (*e.g.* hydrophathy scales<sup>62, 63</sup>). The finding that surprisingly few water structural features are needed to predict interfacial hydrophobicity with high accuracy provides opportunities to quantify the hydrophobicity of complex interfaces (*e.g.*, proteins, colloids, or amphiphile membranes) via more readily accessible experimental measurements of interfacial water structure.<sup>64-66</sup> Our findings further provide a framework to understand how polar group chemistry and patterning modulate hydrophobicity, which could be applied to materials design for the many applications involving water-mediated interactions. We further note that the regression model predicts hydration free energies using water structural features obtained with substantially reduce simulation time compared to INDUS simulations yet achieves comparable accuracy. This computational efficiency indicates that structure-property models based upon water structural features could be utilized as screening tools to rationally fine-tune hydrophobicity, complementing recently developed machine learning techniques<sup>55</sup> by permitting analysis of the importance of water structural features.

## Methods

**SAM models.** Three types of SAMs were modeled in this study: single-component charge-scaled and mixed SAMs with ligands arranged in either a “checkered” or “separated” pattern. Charge-scaled SAMs contained ligands where the partial charges of the end groups were multiplied by a scaling factor,  $k$ , to modify the hydrophobicity of the surface.<sup>23, 55</sup> The two SAM patterns were selected to capture the extremes of possible ligand arrangements. SAMs in the checkered pattern

contained ligands with polar and nonpolar end groups arranged such that the polar end groups were most dispersed on the SAMs. SAMs in the “separated” pattern contained ligands with polar and nonpolar end groups arranged in distinct groups resembling a 2D phase-separated system. All SAMs contained 144 ligands arranged on a  $12 \times 12$  hexagonal lattice to be consistent with a grafting density of  $21.6 \text{ \AA}/\text{ligand}$  to be consistent with experimental measurements for the Au(111) lattice.<sup>67, 68</sup> SAMs were then solvated and periodic boundary conditions were applied to the resulting  $5.2 \times 6.0 \times 11.7 \text{ nm}^3$  SAM-water systems. Ligand atoms were modeled using the CHARMM36 General Force Field (CGenFF-jul2017).<sup>69</sup> Water atoms were modeled using the TIP4P/2005 force field.<sup>70</sup> Additional details of the SAM models are included in ESI Section S1.

***Hydration free energy and water order parameter calculations.*** Two different types of MD simulations were performed for each of the 58 SAMs. INDUS simulations were implemented to calculate the hydration free energies ( $\mu_v$ ) and unbiased simulations were performed to compute water order parameters. Detailed descriptions of both simulation types are provided in ESI Section S1. INDUS was used to quantify the relative hydrophobicity of the SAMs by calculating  $\mu_v$  for a  $2.0 \times 2.0 \times 0.3 \text{ nm}^3$  cuboidal cavity at the SAM-water interface. INDUS applies a biasing harmonic potential to the positions of water molecules in the cavity so that the number of water molecules in the position can be sampled continuously. We biased the number of water molecules inside the cavity using 16 independent simulation windows, each performed for 5 ns (80 ns total). The weighted histogram analysis method (WHAM) was used to compute the unbiased probability distribution of the number of water molecules in the cavity<sup>71</sup> and  $\mu_v$  was obtained via Equation 1:

$$\mu_v = -k_B T \ln p_v(0) \quad (1)$$

$k_B$  is the Boltzmann constant,  $T$  is the temperature, and  $p_v(0)$  is the probability that zero water molecules are within the cavity.

Unbiased simulations were performed for 10 ns and used to compute water order parameters as described in the Results section. Descriptions of the parameters and details about their calculation are include in the ESI Section S2. Water order parameters were only computed for interfacial water molecules, which were defined as all water molecules with a center of mass position within 0.3 nm of the SAM-water interface. Three replicas for both the INDUS and unbiased simulations were used to compute error bars and ensure the robustness of the data-centric feature selection workflow.

### **Conflicts of interests**

There are no conflicts to declare.

### **Acknowledgments**

This work was supported by the National Science Foundation under Grant No. MCB-1817292. This work used the Extreme Science and Engineering Discovery Environment (XSEDE), which is supported by National Science Foundation grant number ACI-1548562. R. C. V. also acknowledges support from the 3M Non-Tenured Faculty Award.



## References

1. K. Lum, D. Chandler and J. D. Weeks, *The Journal of Physical Chemistry B*, 1999, **103**, 4570-4577.
2. D. M. Huang and D. Chandler, *Proc Natl Acad Sci U S A*, 2000, **97**, 8324-8327.
3. D. Chandler, *Nature*, 2005, **437**, 640-647.
4. I. T. Li and G. C. Walker, *Proc Natl Acad Sci U S A*, 2011, **108**, 16527-16532.
5. J. Israelachvili and H. Wennerstrom, *Nature*, 1996, **379**, 219-225.
6. Y. K. Cheng and P. J. Rossky, *Nature*, 1998, **392**, 696-699.
7. M. Kanduc and R. R. Netz, *Proc Natl Acad Sci U S A*, 2015, **112**, 12338-12343.
8. G. Goel, M. V. Athawale, S. Garde and T. M. Truskett, *J Phys Chem B*, 2008, **112**, 13193-13196.
9. H. Yeon, C. Wang, S. H. Gellman and N. L. Abbott, *Molecular Systems Design & Engineering*, 2020, **5**, 835-846.
10. K. A. Dill, *Biochemistry*, 1990, **29**, 7133-7155.
11. C. M. Dobson, *Nature*, 2003, **426**, 884-890.
12. R. E. Beal, D. Toscano-Cantaffa, P. Young, M. Rechsteiner and C. M. Pickart, *Biochemistry*, 1998, **37**, 2925-2934.
13. P. W. Snyder, J. Mecinovic, D. T. Moustakas, S. W. Thomas, 3rd, M. Harder, E. T. Mack, M. R. Lockett, A. Heroux, W. Sherman and G. M. Whitesides, *Proc Natl Acad Sci U S A*, 2011, **108**, 17889-17894.
14. B. Qiao, F. Jimenez-Angeles, T. D. Nguyen and M. Olvera de la Cruz, *Proc Natl Acad Sci U S A*, 2019, **116**, 19274-19281.
15. J. W. Barnett, M. R. Sullivan, J. A. Long, D. Tang, T. Nguyen, D. Ben-Amotz, B. C. Gibb and H. S. Ashbaugh, *Nat Chem*, 2020, **12**, 589-594.
16. T. Cedervall, I. Lynch, S. Lindman, T. Berggard, E. Thulin, H. Nilsson, K. A. Dawson and S. Linse, *Proc Natl Acad Sci U S A*, 2007, **104**, 2050-2055.
17. C. K. Payne, *J Chem Phys*, 2019, **151**, 130901.
18. S. Alamdari and J. Pfaendtner, *Molecular Systems Design & Engineering*, 2020, **5**, 620-631.
19. D. F. Moyano, M. Goldsmith, D. J. Solfiell, D. Landesman-Milo, O. R. Miranda, D. Peer and V. M. Rotello, *J Am Chem Soc*, 2012, **134**, 3965-3967.
20. Y. Jiang, S. Huo, T. Mizuhara, R. Das, Y. W. Lee, S. Hou, D. F. Moyano, B. Duncan, X. J. Liang and V. M. Rotello, *ACS Nano*, 2015, **9**, 9986-9993.
21. D. Rana and T. Matsuura, *Chem Rev*, 2010, **110**, 2448-2471.
22. F. Waibl, M. L. Fernandez-Quintero, A. S. Kamenik, J. Kraml, F. Hofer, H. Kettenberger, G. Georges and K. R. Liedl, *Biophys J*, 2021, **120**, 143-157.
23. N. Giovambattista, P. G. Debenedetti and P. J. Rossky, *J Phys Chem B*, 2007, **111**, 9581-9587.
24. A. J. Patel, P. Varilly, S. N. Jamadagni, H. Acharya, S. Garde and D. Chandler, *Proc Natl Acad Sci U S A*, 2011, **108**, 17678-17683.
25. R. C. Harris and B. M. Pettitt, *Proc Natl Acad Sci U S A*, 2014, **111**, 14681-14686.
26. E. Xi, V. Venkateshwaran, L. Li, N. Rego, A. J. Patel and S. Garde, *Proc Natl Acad Sci U S A*, 2017, **114**, 13345-13350.
27. C. D. Ma, C. Wang, C. Acevedo-Velez, S. H. Gellman and N. L. Abbott, *Nature*, 2015, **517**, 347-350.

28. C. Wang, C. D. Ma, H. Yeon, X. Wang, S. H. Gellman and N. L. Abbott, *J Am Chem Soc*, 2017, **139**, 18536-18544.
29. H. Yeon, C. Wang, R. C. Van Lehn and N. L. Abbott, *Langmuir*, 2017, **33**, 4628-4637.
30. N. B. Rego, E. Xi and A. J. Patel, *Proc Natl Acad Sci U S A*, 2021, **118**.
31. J. A. Reynolds, D. B. Gilbert and C. Tanford, *P Natl Acad Sci USA*, 1974, **71**, 2925-2927.
32. B. C. Stephenson, A. Goldsipe, K. J. Beers and D. Blankschtein, *J Phys Chem B*, 2007, **111**, 1025-1044.
33. L. Jiang, S. Cao, P. P. Cheung, X. Zheng, C. W. T. Leung, Q. Peng, Z. Shuai, B. Z. Tang, S. Yao and X. Huang, *Nat Commun*, 2017, **8**, 15639.
34. J. Chen and C. L. Brooks, 3rd, *Phys Chem Chem Phys*, 2008, **10**, 471-481.
35. C. Chothia, *Nature*, 1974, **248**, 338-339.
36. J. L. MacCallum and D. P. Tieleman, *Trends Biochem Sci*, 2011, **36**, 653-662.
37. X. Li, S. M. Robinson, A. Gupta, K. Saha, Z. Jiang, D. F. Moyano, A. Sahar, M. A. Riley and V. M. Rotello, *ACS Nano*, 2014, **8**, 10682-10686.
38. D. F. Moyano, K. Saha, G. Prakash, B. Yan, H. Kong, M. Yazdani and V. M. Rotello, *ACS Nano*, 2014, **8**, 6748-6755.
39. J. I. Monroe, S. Jiao, R. J. Davis, D. Robinson Brown, L. E. Katz and M. S. Shell, *Proc Natl Acad Sci U S A*, 2021, **118**.
40. S. Gómez, N. Rojas-Valencia, S. A. Gómez, C. Cappelli, G. Merino and A. Restrepo, *Chem Sci*, 2021, **12**, 9233-9245.
41. B. Breiten, M. R. Lockett, W. Sherman, S. Fujita, M. Al-Sayah, H. Lange, C. M. Bowers, A. Heroux, G. Krilov and G. M. Whitesides, *J Am Chem Soc*, 2013, **135**, 15579-15584.
42. C. N. Nguyen, T. K. Young and M. K. Gilson, *J Chem Phys*, 2012, **137**, 044101.
43. J. I. Monroe and M. S. Shell, *Proc Natl Acad Sci U S A*, 2018, **115**, 8093-8098.
44. A. M. Schrader, J. I. Monroe, R. Sheil, H. A. Dobbs, T. J. Keller, Y. Li, S. Jain, M. S. Shell, J. N. Israelachvili and S. Han, *Proc Natl Acad Sci U S A*, 2018, **115**, 2890-2895.
45. R. Godawat, S. N. Jamadagni and S. Garde, *Proc Natl Acad Sci U S A*, 2009, **106**, 15119-15124.
46. H. Acharya, S. Vembanur, S. N. Jamadagni and S. Garde, *Faraday Discuss*, 2010, **146**, 353-365; discussion 367-393, 395-401.
47. A. J. Patel, P. Varilly and D. Chandler, *J Phys Chem B*, 2010, **114**, 1632-1637.
48. A. J. Patel, P. Varilly, S. N. Jamadagni, M. F. Hagan, D. Chandler and S. Garde, *J Phys Chem B*, 2012, **116**, 2498-2503.
49. A. J. Patel and S. Garde, *J Phys Chem B*, 2014, **118**, 1564-1573.
50. T. Young, R. Abel, B. Kim, B. J. Berne and R. A. Friesner, *Proc Natl Acad Sci U S A*, 2007, **104**, 808-813.
51. B. C. Dallin and R. C. Van Lehn, *J Phys Chem Lett*, 2019, **10**, 3991-3997.
52. B. C. Dallin, H. Yeon, A. R. Ostwalt, N. L. Abbott and R. C. Van Lehn, *Langmuir*, 2019, **35**, 2078-2088.
53. A. J. Patel, P. Varilly, D. Chandler and S. Garde, *J Stat Phys*, 2011, **145**, 265-275.
54. A. K. Chew, B. C. Dallin and R. C. Van Lehn, *Acs Nano*, 2021, **15**, 4534-4545.
55. A. S. Kelkar, B. C. Dallin and R. C. Van Lehn, *J Phys Chem B*, 2020, **124**, 9103-9114.
56. T. Head-Gordon and F. H. Stillinger, *The Journal of Chemical Physics*, 1993, **98**, 3313-3327.
57. P. Stock, J. I. Monroe, T. Utzig, D. J. Smith, M. S. Shell and M. Valtiner, *ACS Nano*, 2017, **11**, 2586-2597.

58. J. I. Monroe and M. S. Shell, *J Chem Phys*, 2019, **151**, 094501.
59. M. Kanduc, A. Schlaich, E. Schneck and R. R. Netz, *Langmuir*, 2016, **32**, 8767-8782.
60. A. P. Willard and D. Chandler, *J Chem Phys*, 2014, **141**, 18C519.
61. X. Cui, J. Liu, L. Xie, J. Huang, Q. Liu, J. N. Israelachvili and H. Zeng, *Angew Chem Int Ed Engl*, 2018, **57**, 11903-11908.
62. W. Wei, J. Yu, C. Broomell, J. N. Israelachvili and J. H. Waite, *J Am Chem Soc*, 2013, **135**, 377-383.
63. W. Zheng, G. Dignon, M. Brown, Y. C. Kim and J. Mittal, *J Phys Chem Lett*, 2020, **11**, 3408-3415.
64. L. B. Dreier, Y. Nagata, H. Lutz, G. Gonella, J. Hunger, E. H. G. Backus and M. Bonn, *Sci Adv*, 2018, **4**, eaap7415.
65. J. D. Cyran, M. A. Donovan, D. Vollmer, F. Siro Brigiano, S. Pezzotti, D. R. Galimberti, M. P. Gaigeot, M. Bonn and E. H. G. Backus, *Proc Natl Acad Sci U S A*, 2019, **116**, 1520-1525.
66. J. G. Davis, K. P. Gierszal, P. Wang and D. Ben-Amotz, *Nature*, 2012, **491**, 582-585.
67. M. D. Porter, T. B. Bright, D. L. Allara and C. E. D. Chidsey, *Journal of the American Chemical Society*, 1987, **109**, 3559-3568.
68. J. C. Love, L. A. Estroff, J. K. Kriebel, R. G. Nuzzo and G. M. Whitesides, *Chem Rev*, 2005, **105**, 1103-1169.
69. I. Soteras Gutierrez, F. Y. Lin, K. Vanommeslaeghe, J. A. Lemkul, K. A. Armacost, C. L. Brooks, 3rd and A. D. MacKerell, Jr., *Bioorg Med Chem*, 2016, **24**, 4812-4825.
70. J. L. Abascal and C. Vega, *J Chem Phys*, 2005, **123**, 234505.
71. B. Roux, *Computer Physics Communications*, 1995, **91**, 275-282.